



AFRL-RW-EG-TR-2010-110

## Wireless Telemetry of In-Flight Collision Avoidance Neural Signals in Insects

---

Reid R. Harrison  
Ryan J. Kier

Fabrizio Gabbiani  
Haleh Fotowat  
Raymond Chan

University of Utah

Baylor College of Medicine

Grant No. FA8651-07-1-0007

Sep 2010  
Final Report

**DISTRIBUTION A.** Approved for public release, distribution unlimited. 96<sup>th</sup> ABW/PA Approval and Clearance # 96ABW-2010-0598, dated 07 Dec 2010

**AIR FORCE RESEARCH LABORATORY  
MUNITIONS DIRECTORATE**

## NOTICE AND SIGNATURE PAGE

Using Government drawings, specifications, or other data included in this document for any purpose other than Government procurement does not in any obligate the U.S. Government. The fact that the Government formulated or supplied the drawings, specifications, or other data does not license the holder or any other person or corporation, or convey any rights or permission to manufacture, use, or sell any patented invention that may relate to them.

This report was cleared for public release by the 96<sup>th</sup> Air Base Wing, Public Affairs Office, and is available to the general public, including foreign nationals. Copies may be obtained from the Defense Technical Information Center (DTIC) < <http://www.dtic.mil/dtic/index/html>>.

AFRL-RW-EG-TR-2010-110 HAS BEEN REVIEWED AND IS APPROVED FOR PUBLICATION IN ACCORDANCE WITH ASSIGNED DISTRIBUTION STATEMENT.

FOR THE DIRECTOR:

//ORIGINAL SIGNED//  
ROBERT MURPHEY, PhD, DR-IV  
Acting Technical Director  
Advanced Guidance Division

//ORIGINAL SIGNED//  
PAUL MCCARLEY  
Program Manager

This report is published in the interest of scientific and technical information exchange, and its publication does not constitute the Government's approval or disapproval of its ideas or findings.

REPORT DOCUMENTATION PAGE				Form Approved OMB No. 0704-0188	
Public reporting burden for this collection of information is estimated to average 1 hour per response, including the time for reviewing instructions, searching existing data sources, gathering and maintaining the data needed, and completing and reviewing this collection of information. Send comments regarding this burden estimate or any other aspect of this collection of information, including suggestions for reducing this burden to Department of Defense, Washington Headquarters Services, Directorate for Information Operations and Reports (0704-0188), 1215 Jefferson Davis Highway, Suite 1204, Arlington, VA 22202-4302. Respondents should be aware that notwithstanding any other provision of law, no person shall be subject to any penalty for failing to comply with a collection of information if it does not display a currently valid OMB control number. <b>PLEASE DO NOT RETURN YOUR FORM TO THE ABOVE ADDRESS.</b>					
1. REPORT DATE 13 Sep 2010		2. REPORT TYPE Final		3. DATES COVERED (From - To) (Jul, 2007)-(Aug, 2010)	
4. TITLE AND SUBTITLE  <b>Wireless Telemetry of In-Flight Collision Avoidance Neural Signals in Insects</b>				5a. CONTRACT NUMBER	
				5b. GRANT NUMBER FA8651-07-1-0007	
				5c. PROGRAM ELEMENT NUMBER 62602F	
6. AUTHOR(S) Reid R. Harrison      Fabrizio Gabbiani Ryan J. Kier          Haleh Fotowat Raymond Chan				5d. PROJECT NUMBER 2068	
				5e. TASK NUMBER 99	
				5f. WORK UNIT NUMBER 21	
7. PERFORMING ORGANIZATION NAME(S) AND ADDRESS(ES)  University of Utah      Baylor College of Medicine Salt Lake City, UT      Houston, TX				8. PERFORMING ORGANIZATION REPORT NUMBER	
9. SPONSORING / MONITORING AGENCY NAME(S) AND ADDRESS(ES) Air Force Research Laboratory, Munitions Directorate AFRL/RWGI 101 West Eglin Boulevard Eglin AFB, FL 32542-6810				10. SPONSOR/MONITOR'S ACRONYM(S) AFRL-RW-EG	
				11. SPONSOR/MONITOR'S REPORT NUMBER AFRL-RW-EG-TR-2010-110	
12. DISTRIBUTION / AVAILABILITY STATEMENT DISTRIBUTION A. Approved for public release, distribution unlimited. 96th ABW/PA Approval and Clearance # 96ABW-2010-0598, dated 07 Dec 2010					
13. SUPPLEMENTARY NOTES					
14. ABSTRACT Modern neuroscience research often relies on experiments using small animals such as mice and insects. For example, flying insects possess highly capable visual systems that perform complex, real time calculations to modulate flight control. The study of insect visual processing during the past half century has provided rich insight into biological information processing strategies. Measuring the weak extracellular electrical activity produced by neurons or electromyograms (EMGs) in muscles by traditional means has required large rack-mounted amplifiers and data acquisition systems. Due to the long wires connecting electrodes to remote amplifiers, most electrophysiology experiments must be performed inside a Faraday cage to achieve acceptable signal quality. Animals must be head-fixed or tethered during these experiments, which restricts the simultaneous study of neural activity and behavior.  As electronics have been miniaturized, efforts have been made to create small, lightweight amplifiers and wireless transmitters to permit electrophysiological monitoring during free behavior. Early designs used discrete components to provide analog telemetry of EMG signals from large flying moths. Simple RF beacons have been used to track dragonfly migration. More recently, integrated circuits have been used to increase functionality (e.g., stimulating neurons in flying moths). To facilitate more sophisticated investigations into the neural control of behavior, we have developed an integrated circuit capable of amplifying two neural signals and two EMG signals from extracellular electrodes, digitizing these signals, adding parity bits for error detection, and wirelessly transmitting the digital information while operating from small, low-mass batteries.					
15. SUBJECT TERMS Insect vision, neural signal recording.					
16. SECURITY CLASSIFICATION OF:			17. LIMITATION OF ABSTRACT  UL	18. NUMBER OF PAGES  20	19a. NAME OF RESPONSIBLE PERSON Paul McCarley
a. REPORT  UNCLASSIFIED	b. ABSTRACT  UNCLASSIFIED	c. THIS PAGE  UNCLASSIFIED			19b. TELEPHONE NUMBER (include area code) 850-883-0889

## Table of Contents

List of Figures.....	ii
I. Introduction .....	1
II. Telemetry System Design.....	1
Integrated Circuit Design.....	1
System-Level Design.....	2
III. Experimental Results.....	4
Recording from Dragonfly Nerve Cord.....	4
Recording from Freely Jumping Locust .....	4
Results .....	6
Recording from Loosely-Tethered Flying Locust .....	11
IV. Discussion .....	14
V. Next-Generation Wireless Recording System .....	16
VI. References .....	17

## LIST OF FIGURES

FIGURE 1.	SCHEMATIC OF LOW-NOISE BIOPOTENTIAL AMPLIFIER.	2
FIGURE 2.	SCHEMATIC OF 920-MHZ FSK TRANSMITTER.	2
FIGURE 3.	DIE PHOTO OF 2.57 X 2.48MM <sup>2</sup> INSECT TELEMETRY CHIP.	3
FIGURE 4.	(A) COMPLETE 13 X 9 MM <sup>2</sup> TELEMETRY SYSTEM. (B) SIDE VIEW OF TELEMETRY SYSTEM SHOWING ACCELEROMETER AND CRYSTAL.	3
FIGURE 5.	(A) EXTRACELLULAR RECORDING OF SPIKING ACTIVITY FROM NEURON MDT1 IN THE DRAGONFLY NERVE CORD, (B) CLOSE-UP COMPARISON OF THREE SPIKES.	3
FIGURE 6.	TELEMETRY SYSTEM MOUNTED ON A LOCUST <i>SCHISTOCERCA AMERICANA</i> .	5
FIGURE 7.	NEURAL, MUSCLE, AND ACCELERATION RECORDINGS OBTAINED DURING JUMP BEHAVIOR.	5
FIGURE 8.	RELATIVE TIMING OF JUMP-ESCAPE STAGES IN FREELY BEHAVING ANIMALS.	
FIGURE 9.	NEURAL AND MUSCLE RECORDINGS DURING A TRIAL IN WHICH THE ANIMAL DID NOT TAKE OFF.	7
FIGURE 10.	COMPARISON BETWEEN SENSORY AND MOTOR ACTIVITY IN JUMP (J) AND NO JUMP (NJ) TRIALS.	9
FIGURE 11.	PREDICTING TAKE-OFF FROM SENSORY AND MOTOR ATTRIBUTES.	9
FIGURE 12.	A DCMD FIRING RATE THRESHOLD CONTRIBUTES TO TRIGGERING CO-CONTRACTION.	10
FIGURE 13.	SIDE VIEWS OF THE WIND TUNNEL AND OF THE EQUIPMENT USED TO FILM THE ANIMALS.	11
FIGURE 14.	STIMULI GENERATED ON THE REAR PROJECTION SCREEN.	12
FIGURE 15.	ANIMAL'S TRAJECTORY DURING A LOOMING STIMULUS PRESENTATION.	12
FIGURE 16.	TWO DIMENSIONAL PLOTS OF THE ANIMAL'S TRAJECTORY.	13
FIGURE 17.	HISTOGRAM OF THE COLLISION AVOIDANCE BEHAVIORS.	13
FIGURE 18.	TIME AT WHICH SIX DIFFERENT TYPES OF AVOIDANCE BEHAVIORS OCCUR DURING A TRIAL.	13
FIGURE 19.	TRAJECTORY OF THE LEFT AND RIGHT FOREWING TIPS IN THE VERTICAL PLANE.	14
FIGURE 20.	PHOTOGRAPH OF LIVE WIRELESS DATA ACQUISITION FROM LOCUST FLYING IN WIND TUNNEL.	14
FIGURE 21.	DATA OBTAINED WIRELESSLY FROM A LOOSELY TETHERED LOCUST FLYING IN A WIND TUNNEL.	14
FIGURE 22.	CUSTOM WIRELESS TELEMETRY RECEIVER WITH USB INTERFACE TO PC.	16
FIGURE 23.	FIRST-GENERATION WIRELESS TELEMETRY SYSTEM WEIGHING 790 MG (LEFT); NEXT-GENERATION SYSTEM WEIGHING 266 MG (RIGHT).	16

## I. INTRODUCTION

Modern neuroscience research often relies on experiments using small animals such as mice and insects. For example, flying insects possess highly capable visual systems that perform complex, real time calculations to modulate flight control (see Olberg et al., 2007, and references therein). The study of insect visual processing during the past half century has provided rich insight into biological information processing strategies.

Measuring the weak extracellular electrical activity produced by neurons (typically in the range of 100  $\mu\text{V}$  - 1 mV) or electromyograms (EMGs) in muscles (typically in the range of 1-10 mV) by traditional means has required large rack-mounted amplifiers and data acquisition systems. Due to the long wires connecting electrodes to remote amplifiers, most electrophysiology experiments must be performed inside a Faraday cage to achieve acceptable signal quality. Animals must be head-fixed or tethered during these experiments, which restricts the simultaneous study of neural activity and behavior.

As electronics have been miniaturized, efforts have been made to create small, lightweight amplifiers and wireless transmitters to permit electrophysiological monitoring during free behavior. Early designs used discrete components to provide analog telemetry of EMG signals from large flying moths (Kutsch et al., 1993; Kuwana et al., 1999). Simple RF beacons have been used to track dragonfly migration (Wikelski et al., 2006). More recently, integrated circuits have been used to increase functionality (e.g., stimulating neurons in flying moths [Mavoori et al., 2004; Daly et al., 2009]). To facilitate more sophisticated investigations into the neural control of behavior, we have developed an integrated circuit capable of amplifying two neural signals and two EMG signals from extracellular electrodes, digitizing these signals, adding parity bits for error detection, and wirelessly transmitting the digital information while operating from small, low-mass batteries.

This project was divided between Reid Harrison's lab at the University of Utah (Salt Lake City, Utah) and Fabrizio Gabbiani's lab at Baylor College of Medicine (Houston, Texas). All chip and circuit development was done at the University of Utah, which was the lead institution on this grant. All insect experiments were performed at Baylor College of Medicine under a subcontract.

## II. TELEMETRY SYSTEM DESIGN

### Integrated Circuit Design

We designed a custom integrated circuit for the telemetry system in a commercially available 0.6- $\mu\text{m}$  BiCMOS (bipolar/complementary metal-oxide semiconductor) process. Using low-mass batteries imposes severe power limits on the design of the chip: small batteries have low capacities and high internal resistance; pulling too much current can cause a battery's voltage to collapse immediately, regardless of its capacity. After testing many battery types, we opted to use 1.5V silver oxide batteries (Energizer 337) having a mass of 130 mg each and a volume of 29  $\text{mm}^3$ . While these batteries have a stated capacity of 8.3 mAh, drawing 1 mA from the battery reduces its capacity to 3 mAh. Currents greater than 2 mA cause large drops in battery voltage and cannot be used. We use two batteries to provide a 3.0V supply.

Four fully-integrated low-noise amplifiers (see Fig. 1) are used to boost and filter the neural and EMG signals obtained from differential electrodes. Three operational transconductance amplifiers (OTAs) used in the circuit are current-mirror OTAs designed for low-noise operation by proper sizing of differential pair and current mirror transistors (Harrison and Charles, 2003). The gain of the first stage is set by the  $C_1/C_2$  ratio; the second-stage gain is set by  $C_3/C_4$ . Bias generators set the high-frequency cutoff (through  $G_{m1}$  and  $G_{m2}$ ) and low-frequency cutoff (through  $G_{m3}$ ) of each amplifier. The  $G_{m3}$  OTA was placed in the second stage so its noise contribution is attenuated by  $C_1/C_2$  when referred to the input (Harrison, 2008). The gain of the EMG amplifiers was set to 100; the gain of the neural amplifiers was set to 1000. Measured CMRR (common-mode rejection ratio) at 1 kHz (averaged across 10 amplifiers) was 74 dB; PSRR (power supply rejection ratio) was 63 dB.

A 9-bit successive-approximation register (SAR) analog-to-digital converter (ADC) with capacitive digital-to-analog converter (DAC) is used to digitize the amplified waveforms. A state machine controls an analog multiplexer and samples the neural signals at a faster rate (11.52 kS/s) than the slower EMG signals (1.92 kS/s). The ADC also samples (at 1.92 kS/s) three auxiliary input pins that are used to interface a commercially-available 3-axis MEMS accelerometer (Analog Devices ADXL330) with the chip to provide information on insect movement. The sampling rates are set by a low-power crystal oscillator using an off-chip 11.0592 MHz quartz crystal and drawing only 65  $\mu\text{A}$  from the supply. For every 9-bit sample a parity bit is added to permit error detection. Frame marker bits are added, and the resulting 345.6 kb/s serial bit stream is passed to an on-chip frequency-shift keying (FSK) transmitter (see Fig. 2). Table I summarizes the dynamic range, bandwidth, sampling rate, and input-referred noise of each channel.

The core of the 920-MHz transmitter is an  $LC$  oscillator that uses a thick top metal layer to build a low-loss 26 nH inductor  $L_o$  ( $Q \approx 11$ ). The use of a tank with a high  $LQ$  product, along with vertical  $nnp$  transistors ( $Q_1$  and  $Q_2$ ) providing a high  $g_m/I$  ratio with relatively low parasitic capacitance allows this circuit to oscillate reliably with a bias current of only 180  $\mu$ A. Small MOS varactors ( $M_o$ ) are used to create a 600 kHz frequency deviation in response to a binary input. To save power, a phase-locked-loop (PLL) was not implemented and the oscillator operates in open loop. The measured frequency drift with supply voltage was -2.8 ppm/mV. The batteries have a very flat discharge curve, so frequency drift over time is measureable but not severe. A differential RF output stage with on-chip drain inductors and series capacitors is connected to an off-chip dipole antenna. Off-chip 56-nH inductors are used to improve radiation from the electrically short dipole. A die photograph of the  $2.57 \times 2.48 \text{ mm}^2$  chip is shown in Fig. 3.

### System-Level Design

Chips were packaged in a molded plastic 28-lead  $5 \times 5 \text{ mm}^2$  QFN (quad flat, no leads) package and mounted on a  $13 \times 9 \text{ mm}^2$  printed circuit board (PCB) along with battery holders, accelerometer, crystal, and antenna (see Fig. 4). The complete system with batteries weighs 0.79 g. The chip consumes 880  $\mu$ A of current and the accelerometer consumes 320  $\mu$ A, for a total of 1.2 mA. This limits battery life to 2 h of continuous use. The telemetry system can be temporarily mounted to an insect using wax, and electrode wires are soldered to the PCB.

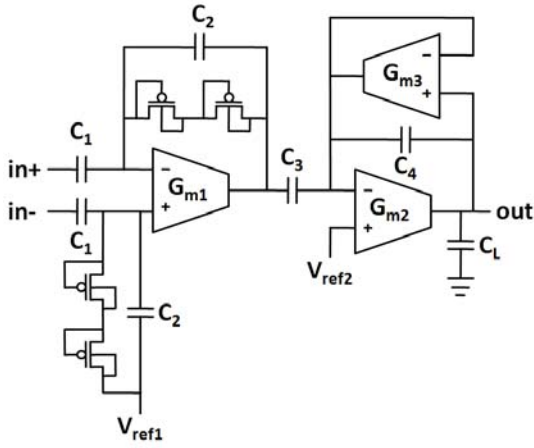


Figure 1. Schematic of low-noise biopotential amplifier. Operational transconductance amplifiers (OTAs) are designed according to Harrison and Charles, 2003.

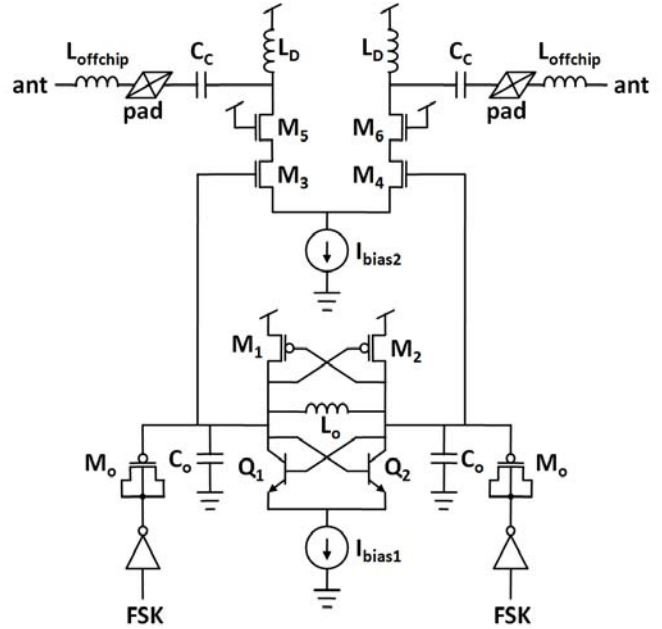


Figure 2. Schematic of 920-MHz FSK transmitter. Varactors ( $M_o$ ) shift the resonant frequency of an open-loop negative-resistance  $LC$  oscillator.

TABLE I. TELEMETRY CHANNEL SPECIFICATIONS

Data Channel	Band-width	ADC Sampling Rate	Max. Range	ADC $V_{LSB}$	Input-Referred Noise
Neural Amps 1,2	300Hz-5.2kHz	11.52 kS/s	$\pm 1.2\text{mV}$	$4.69\mu\text{V}$	$2.3\mu\text{V}_{\text{rms}}$
EMG Amps 1,2	20Hz-280Hz	1.92 kS/s	$\pm 12\text{mV}$	$46.9\mu\text{V}$	$25\mu\text{V}_{\text{rms}}$
Acceler. X,Y,Z	DC-500 Hz	1.92 kS/s	$\pm 3.0\text{g}^1$	$15.6\text{mg}$	$7.8\text{mg}_{\text{rms}}$ (X,Y) $9.8\text{mg}_{\text{rms}}$ (Z)

<sup>1</sup>  $1\text{ g} = 9.81\text{ m/s}^2$

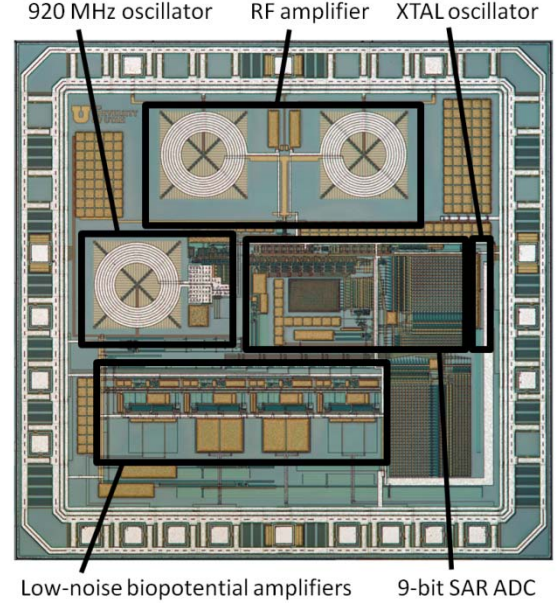


Figure 3. Die photo of  $2.57 \times 2.48\text{mm}^2$  insect telemetry chip, fabricated in a  $0.6\text{-}\mu\text{m}$  BiCMOS process.

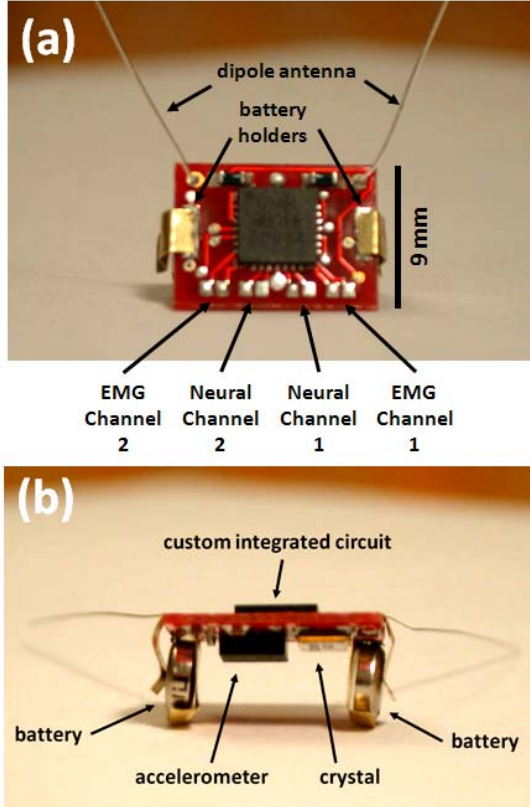


Figure 4. (a) Complete  $13 \times 9\text{mm}^2$  telemetry system with QFN-packaged chip. (b) Side view of telemetry system showing accelerometer and crystal.

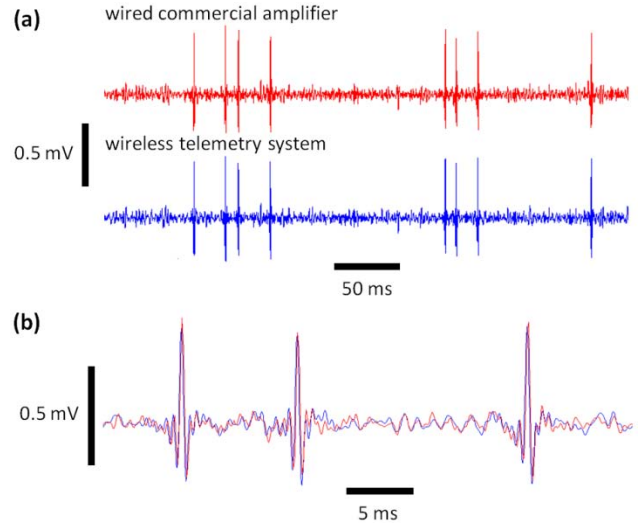


Figure 5. (a) Extracellular recording of spiking activity from neuron MDT1 in the dragonfly nerve cord, using wired commercial amplifier (red) and wireless telemetry system (blue). (b) Close-up comparison of three spikes.

### III. EXPERIMENTAL RESULTS

#### Recording from Dragonfly Nerve Cord

In a side collaboration with Dr. Anthony Leonardo at the Howard Hughes Medical Institute's Janelia Farm Research Campus (JFRC) in Ashburn, Virginia, we performed initial tests of the telemetry system by recording neural activity from the target selective descending neuron MDT1 in the ventral nerve cord of a restrained dragonfly. A single 1.2 M $\Omega$  tungsten electrode was simultaneously monitored using a conventional wired amplifier (AM Systems 3600, 40 kHz sampling) and a neural amplifier channel from the wireless telemetry unit (see Fig. 5). The data matched very closely. A background noise level of 11.5  $\mu$ V<sub>rms</sub> was observed using the wired amplifier, while 12.1  $\mu$ V<sub>rms</sub> was observed using the wireless telemetry unit (over a bandwidth of 300 Hz to 5 kHz). These results were valuable for confirming reliable and accurate operation of the system with real insect neurons.

#### Recording from Freely Jumping Locust

At Baylor, Gabbiani's group used the telemetry system to investigate the transformation of sensory signals into motor commands leading to escape behaviors. Such transformations play a pivotal role in the generation of behavior and much work, both in vertebrates and invertebrates, has focused on characterizing how the spike trains of sensory neurons may determine the motor output of an organism (Mountcastle et al. 1975; Newsome et al., 1988; Trimarchi and Schneidman, 1993; Lewis and Kristan, 1998; Edwards et al., 1999; van Hateren et al., 2005; Santer et al., 2006; Marsat and Pollack 2006; Lima and Miesenböck 2005; Korn and Faber, 2005; Ishikane et al., 2005; De Lafuente and Romo, 2005; Gu et al., 2008; Cohen and Newsome, 2009; Nienborg and Cummings, 2009). In particular, both the mean number of spikes, and firing rate thresholds in sensory neuron populations were implicated in determining behavior (Camhi and Levy, 1989; Cook and Maunsell, 2002; Roitman and Shadlen, 2002). Yet, the precise algorithms used by the brain to initiate specific motor sequences and the size of the neuronal pools involved remains under debate.

Collision avoidance and escape behaviors are critical for survival. Specialized neural circuits implementing them have been studied in several species (Wang and Frost, 1992; Graziano et al., 1994; Wicklein and Strausfeld, 2000; Yamamoto et al., 2003; Preuss et al., 2006; Olivia et al., 2007; Fotowat et al., 2009). In locusts, the third neuropil in each of the two optic lobes contains an identified neuron, the lobula giant movement detector (LGMD) that responds specifically to objects approaching on a collision course in its associated visual hemifield, or their two-dimensional projection: looming stimuli (Hatsopoulos et al., 1995; Schlotterer, 1977; Rind and Simmons, 1992; Judge and Rind, 1997; Peron and Gabbiani, 2009). (A 'neuropil' is a region of the nervous system where synaptic connections are formed between branches of axons and dendrites or cell bodies.) Each LGMD synapses in the brain onto the descending contralateral movement detector (DCMD) neuron, such that their spikes are in one-to-one correspondence (Rind, 1984; Killmann and Schurmann, 1985). In response to looming stimuli the firing rate of these neurons gradually increases, peaks, and rapidly decreases before expected collision (Gabbiani et al., 1999). Similar response profiles have now been described in neurons of wide-ranging species (pigeon: Sun and Frost, 1998; frog: Kang and Nakagawa, 2006; fish: Preuss et al., 2006; fruit fly: Fotowat et al., 2009). In locusts, this response profile is robust to a broad spectrum of stimulus changes, suggesting that it may play an important role in the generation of escape behaviors (Gabbiani et al., 2001).

From the brain, each DCMD axon projects through the contralateral nerve cord to motor centers involved in jump and flight steering (O'Shea et al. 1974; Simmons, 1980). In particular, the DCMDs make both direct and indirect synaptic contacts with the Fast Extensor Tibia (FETi) motoneuron of the hind leg, and indirect connections to the flexor tibia motoneurons (Burrows and Rowell, 1973; Pearson et al., 1980; Pearson and Robertson, 1981).

The involvement of DCMD activity in jump escape behaviors has been studied, but its role remains unclear (Fotowat and Gabbiani, 2007; Burrows, 1996; Santer et al., 2005). Up to now, it was impossible to record simultaneously from the DCMD and motoneurons during freely executed, visually guided jump escape behaviors. Consequently, it was not possible to observe how sensory and motor activities are related on a trial-by-trial basis. To achieve this goal, we used the telemetry system built at the University of Utah (described above). This system was sufficiently small that locusts could carry it as a backpack (see Fig. 6) and still respond to looming stimuli by jumping.

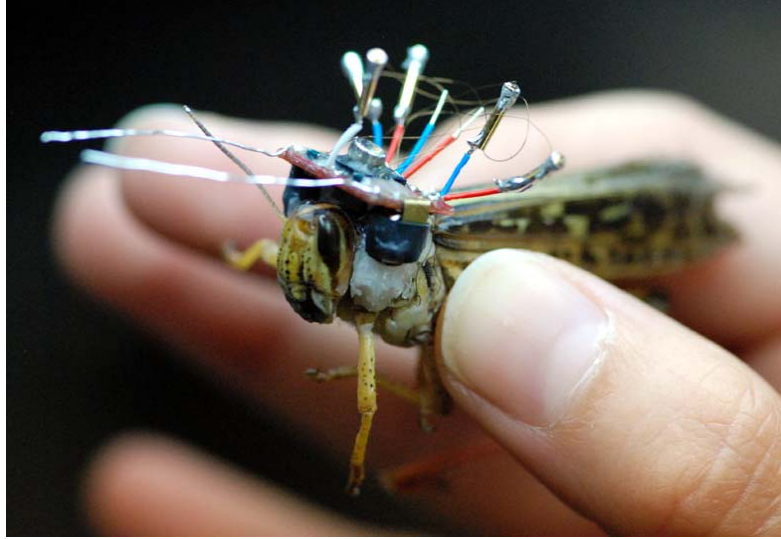


Figure 6. Telemetry system mounted on a locust *Schistocerca americana*.

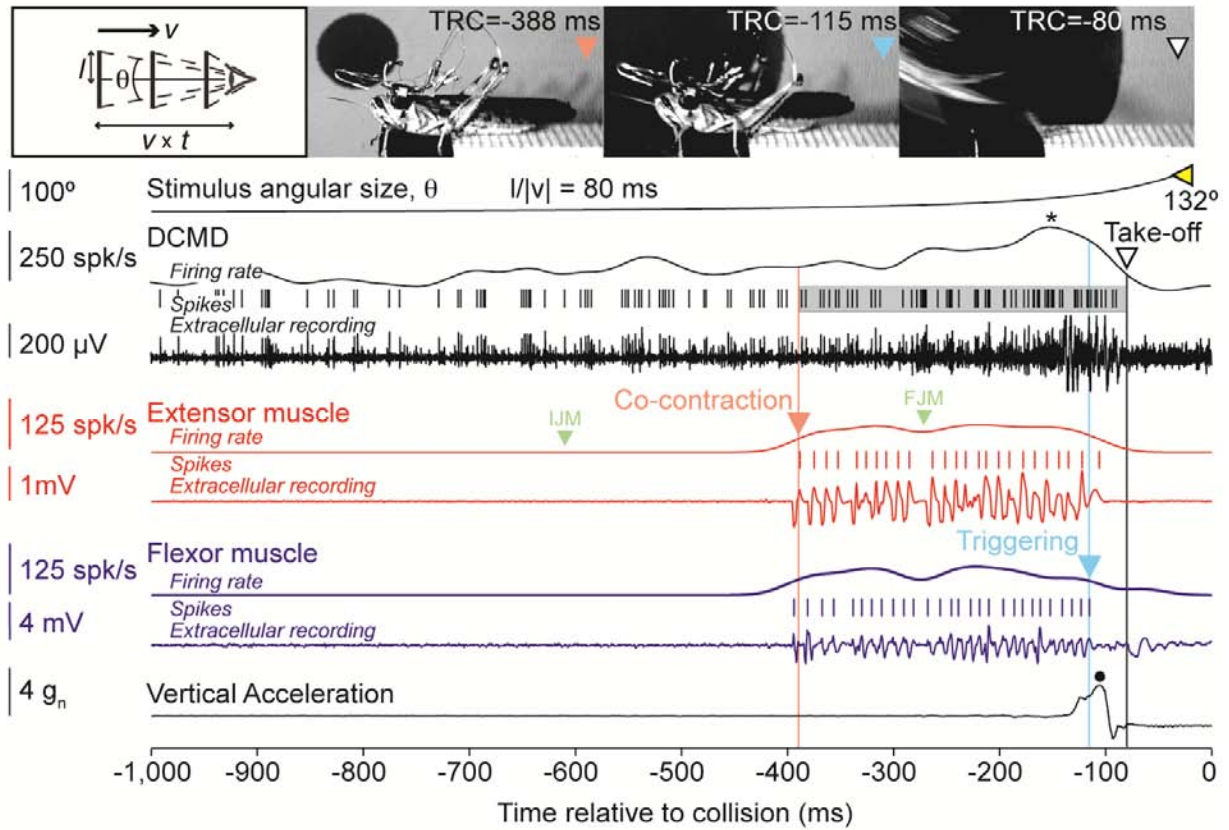


Figure 7. Neural, muscle, and acceleration recordings obtained during jump behavior using wireless telemetry. Time markers and corresponding video frames for the onset of co-contraction, its end (triggering), and take-off are indicated with  $\blacktriangle$ ,  $\blacktriangledown$ , and  $\blacktriangledown$ , respectively;  $\blacktriangle$  marks the final angular size. The timing of the Initial and Final Joint Movements (IJM and FJM) are marked by the symbols [  $\blacktriangledown$  ] (see Results). Co-contraction starts before, and take-off occurs after the peak (\*) DCMD firing rate (TRC= Time Relative to Collision). The shaded area around the DCMD spikes corresponds to the time period over which they were counted for further analysis (see Results). The right and left bounds of the shaded area are the co-contraction onset and take-off time, respectively. Peak vertical acceleration marked by a  $\bullet$ . Top left inset: Schematics of the stimuli. Discs of radius  $l$  approaching at constant speed  $v$  subtend an angle  $\theta$  at the retina. By convention  $v < 0$  for approaching objects and  $t < 0$  before collision (bottom axis).  $(v \times t)$  is the distance of the object to the eye.

## Results

Our digital telemetry system allowed us to monitor simultaneously the sensory and motor activity evoked by looming stimuli during collision avoidance behaviors. The simulated objects were black discs on a bright background with various size to speed ratios,  $l/|v|$ , where  $l$  is the disc radius and  $|v|$  the approach speed. The size to speed ratio, in units of time, determines the stimulus angular size,  $\theta(t)$ , since by trigonometry the tangent of  $\theta/2$  is the ratio of  $l$  to the object's distance ( $v \times t$ ; Fig. 7). Equivalently,  $l/|v|$  is the time remaining to collision when the stimulus subtends  $90^\circ$  on the retina. Thus, the faster the stimulus approach speed,  $|v|$ , the smaller  $l/|v|$ . Looming stimuli were always presented on one side of the animal so that a single DCMD neuron was stimulated.

### *Energy storage starts before, and take-off occurs after peak DCMD firing rate*

Fig. 7 shows a trial in which a locust jumped in response to a looming stimulus. Spikes from the DCMD, the Fast Extensor Tibiae (FETi) and flexor motoneurons were obtained by extracellular recording from the contralateral nerve cord, the hind leg extensor and flexor muscles, respectively. The time course of the vertical acceleration was measured by an on-board accelerometer. The locust jump is a complex behavior, consisting of several distinct phases, during which the animal orients itself away from the approaching object using its middle legs and stores the energy required for take-off in the elastic elements of its hind legs (Burrows, 1996; Santer et al., 2005). By monitoring the position of the hind leg femur-tibia joint, we previously showed that after an initial flexion of the tibia, the joint moves to align the leg parallel to the body (initial joint movement, IJM; Fotowat and Gabbiani, 2007). Subsequently, the flexor and extensor muscles contract simultaneously to store the mechanical energy required for the jump (co-contraction). This leads to a final femur-tibia joint movement (FJM), which is followed by cessation of activity in the flexors (triggering) that allows energy release and take-off. Looming stimuli with  $l/|v|$  values larger than 40 ms led to jumps before the expected collision time. As illustrated in Fig. 7, locusts started to accelerate towards the end of co-contraction, with the peak vertical acceleration occurring immediately after triggering (mean:  $5.8 g_n$ , SD: 1.3; number of locusts,  $n_L = 3$ , number of trials,  $n_T = 20$ ). During co-contraction the flexors and extensors fired fairly regular spike trains (mean ISI: 14 ms, CV: 0.69,  $n_L = 4$ ,  $n_T = 54$ ), and the number of their spikes were highly correlated ( $\rho=0.8$ ,  $p < 10^{-9}$ ). The DCMD firing rate gradually increased, peaked, and sharply decreased before projected collision, as observed in fixed animals (Fotowat and Gabbiani, 2007). Fig. 7 shows that the co-contraction phase started before the DCMD firing rate reached its peak (mean: 169 ms, SD: 49,  $n_L = 3$ ,  $n_T = 24$ ), whereas take-off occurred afterward. This was the case in every trial for all animals (Fig. 8A).

Which aspects of the motor and sensory activity determine the timing of the jump? We found that the time at which the co-contraction ended (triggering) was highly correlated with take-off ( $\rho = 0.95$ ,  $p < 10^{-9}$ ). Moreover, this correlation exists regardless of  $l/|v|$ , since the partial correlation coefficient between these two variables controlling for  $l/|v|$  remained high ( $\rho_{\text{part}} = 0.94$ ,  $p < 10^{-9}$ ). On average take-off occurred 36 ms after triggering (SD: 15,  $n_L = 4$ ,  $n_T = 29$ ; Fig. 8B, dashed line) and 90% of the variance in the timing of take-off could be explained by the timing of triggering. At the sensory level, we found that the timing of the DCMD peak firing rate and take-off were highly correlated as well ( $\rho = 0.87$ ,  $p < 10^{-9}$ ) and that the partial correlation coefficient between these variables controlling for  $l/|v|$  also remained high ( $\rho_{\text{part}} = 0.73$ ,  $p = 9.2 \times 10^{-8}$ ). Locusts took off on average 70 ms (SD: 13) after the DCMD firing rate peaked, regardless of the stimulus size to speed ratio (Fig. 8C, dashed line) and the timing of the peak accounted for 75% of the variance of the take-off time. Whereas the timing of the DCMD peak significantly affected the timing of take-off, it could not affect the timing of co-contraction onset, which always occurred earlier.

### *Comparison of sensory-motor activity in trials with and without jump*

Not all looming stimuli led to a final take-off. Thus, locusts jumped with a median probability of 32%. The jump probability was significantly reduced compared to that of animals without a telemetry backpack (Fotowat and Gabbiani, 2007; median: 64%,  $p_{\text{KWT}}=0.003$ ). Fig. 9 shows a trial in which the same locust as in Fig. 7 did not jump. It started preparing by co-contracting its hind leg flexor and extensor muscles. However, compared to jump trials, the co-contraction started late, such that after a few spikes in the extensor the looming stimulus reached its full size, the DCMD firing rate declined, and the co-contraction ended. This was the case in 85% of trials without take-off, whereas in the remaining 15% the co-contraction failed to initiate altogether.

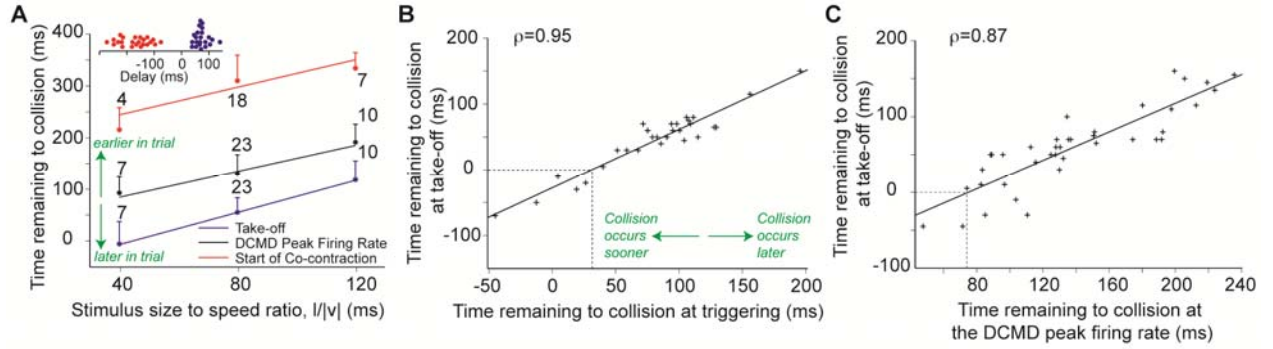


Figure 8. Relative timing of jump-escape stages in freely behaving animals. **A**) Timing of co-contraction onset (red), DCMD peak firing rate (black) and take-off (blue) in response to looming stimuli with  $l/|v| = 40, 80$ , and  $120$  ms ( $n_T$  shown on figure). The timing of these stages was highly correlated with  $l/|v|$ ,  $\rho = 0.57, 0.69$ , and  $0.78$ , respectively. Slopes ( $\alpha$ ) and intercepts ( $\delta$ ) of linear fits were as follows. Start of co-contraction:  $\alpha = 1.33$  (SD:  $0.37$ ),  $\delta = 191$  ms (SD:  $33$ ); DCMD peak:  $\alpha = 1.26$  (SD:  $0.22$ ),  $\delta = 34$  ms (SD:  $19$ ); Take-off:  $\alpha = 1.55$  (SD:  $0.20$ ),  $\delta = -69$  ms (SD:  $18$ ). Top inset: Representative delays between DCMD peak and co-contraction onset (red) and between peak and take-off (blue;  $n_T = 23$ ). Positive delays correspond to events after the peak (data points staggered vertically for clarity). **B**) The end of co-contraction (triggering) and take-off were highly correlated ( $\rho = 0.95$ , data pooled across  $l/|v|$  values). Linear fit slope:  $0.89$  (SD:  $0.06$ ); intercept:  $-27$  ms (SD:  $3.7$ ), indicating that take-off occurs approximately  $27$  ms after triggering (dashed line). **C**) Timing of DCMD peak firing rate and take-off relative to expected collision time were highly correlated ( $\rho = 0.87$ , data pooled across  $l/|v|$  values). Linear fit slope:  $0.94$  (SD:  $0.09$ ); intercept:  $-70$  ms (SD:  $13$ ), indicating that take-off occurs approximately  $70$  ms after the DCMD peak (dashed line).  $n_L = 9$  for DCMD and take-off data,  $n_L = 4$  for co-contraction data.

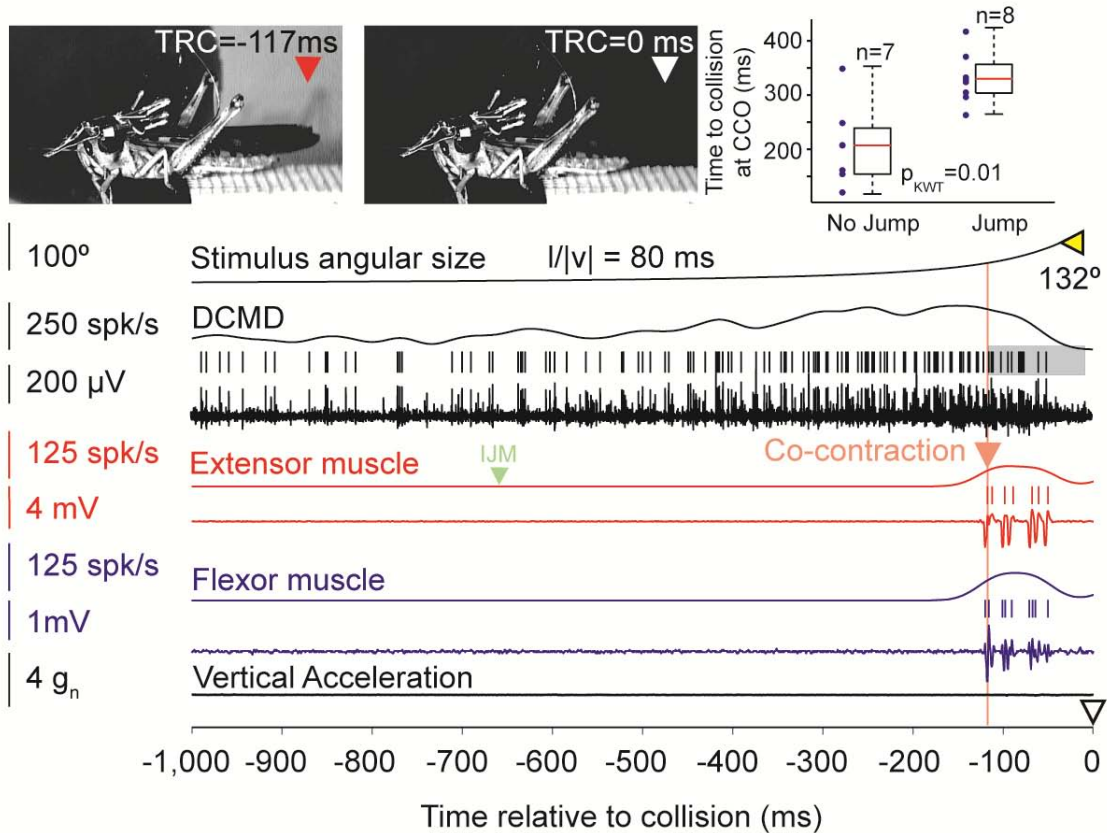


Figure 9. Neural and muscle recordings during a trial in which the animal did not take off. The symbols  $\blacktriangledown$  and  $\blacktriangledown$  mark the start of co-contraction, and the expected collision time, respectively (and corresponding video frames);  $\blacktriangle$  marks the final angular size. The locust prepares to jump by co-contracting its flexor and extensor muscles, but never takes off (same animal as in Fig. 7). The shaded area around the DCMD spikes corresponds to the time period over which they were counted for further analysis (see Results). The right and left bounds are the co-contraction onset and the time at which the DCMD firing rate falls below 5 spk/s respectively. Top right: Co-contraction onset (CCO) occurred significantly earlier for jumps (all trials at  $l/|v| = 80$  ms, same locust as in main panel). Individual trial values shown on left (dots); corresponding box plots on right.

Across animals, we found that the co-contraction onset occurred significantly earlier relative to collision in jump trials (Fig. 10A), whereas the timing of the DCMD peak itself did not change (Fig. 10B). Thus, while the DCMD peak time predicts the time of take-off, it fails to predict its occurrence. Since co-contraction started earlier in jump trials, the number of extensor spikes was also significantly higher (Fig. 10C). In contrast, there was no difference in the total number of DCMD spikes between jump and no-jump trials (Fig. 10D), although the peak DCMD firing rate was higher in jump trials. However, we found that if we started counting the DCMD spikes from co-contraction onset rather than stimulus onset (shaded areas in Figs. 1 and 3), their number was significantly higher in jump trials (Fig. 10E). Furthermore, the number of DCMD spikes from co-contraction onset was highly correlated with the number of extensor spikes ( $\rho = 0.73$ ,  $p < 10^{-9}$ , Fig. 10F), such that on average 4.3 DCMD spikes led to one extensor spike (SD: 2.1 spk). To test for a causal relation between the DCMD and extensor firing rates following co-contraction onset, we designed looming stimuli that abruptly stopped in mid-course and resumed their looming immediately thereafter. This often caused the DCMD firing rate to peak twice: once before and once after the abrupt motion cessation (in 13 out of 17 trials,  $n_L = 3$ ). Under these conditions, the firing rate in the extensor faithfully tracked that of the DCMD in 10 of these 13 trials. Of the remaining 3 trials, 2 failed to elicit extensor spikes, while the last one elicited spikes only after the second DCMD peak.

Which motor or sensory attribute best predicts the occurrence of a jump? To address this question we trained a naïve Bayes classifier to discriminate between jump and no-jump trials based on various sensory and motor attributes (Fig. 11). The number of extensor spikes predicted the occurrence of a jump with an accuracy of 70% (SD: 7%). The time of co-contraction onset did even better (83%, SD: 4%). On the sensory side, the number of DCMD spikes after co-contraction onset had a similar accuracy (82%, SD: 6%). In contrast, DCMD attributes computed before co-contraction onset consistently performed poorly. Although several other attributes predicted the occurrence of a jump, none did as well as the time of co-contraction onset or the number of DCMD spikes after co-contraction onset. In particular, the variability of the DCMD spike train, as embodied by the standard deviation of its inter-spike interval (ISI) distribution, could predict a substantial fraction of the jumps, but it did not improve the prediction accuracy given by the number of DCMD spikes after co-contraction onset. On the other hand, adding information about the mean or SD of the DCMD ISI to the number of extensor spikes, significantly improved the performance of the classifier (Fig. 8C, attributes 7 and 8). It is therefore likely that the increase in the number of DCMD spikes (and a concurrent decrease in the mean and SD of the ISI) results in better summation of these spikes in the FETi and other thoracic interneurons.

### *Co-contraction is triggered a fixed delay after a threshold DCMD firing rate*

We next asked which aspect of the DCMD firing pattern could play a role in triggering the co-contraction. Both the timing of co-contraction (Fig. 10A), and a threshold in the DCMD firing rate vary linearly with  $1/|v|$  (Gabbiani et al., 2002). We therefore investigated whether a threshold in the DCMD firing rate could trigger the co-contraction using three different approaches. First, we presented locusts with looming stimuli stopping at various final sizes. Stopping the stimulus at smaller final sizes allowed us to reduce excitation to the DCMD before it peaks, and therefore manipulate its maximum firing rate (Gabbiani et al., 2005). Fig. 12A shows the DCMD and extensor muscle activity evoked in response to such stimuli. At the lowest final size no extensor spikes were recorded. Increasingly larger final sizes caused a concurrent increase in the DCMD maximal firing rate and the number of extensor spikes. While final angular size was not always a strong predictor of the occurrence of co-contraction, the probability distribution of the DCMD maximum firing rate for trials with co-contraction was shifted to larger firing rates compared to trials without co-contraction (Fig. 12B). Using a linear discriminant, we could predict with an accuracy of 83% the occurrence of co-contraction based on whether the maximum DCMD firing rate exceeded 248 spk/s. Second, in a subset of these trials ( $n_T = 9$ ,  $n_L = 6$ ) only one or two extensor spikes were recorded after the stimulus had stopped and the DCMD had reached its maximum activity. Thus, the maximum DCMD activity in these trials, 300 spk/s on average, was just above the threshold required to trigger the co-contraction (SD: 72). This value is close to that suggested to trigger collision avoidance in flight (Santer et al., 2006) and not significantly higher than that estimated using a linear discriminant (t-test,  $p = 0.073$ ). Furthermore, in these trials the average delay between the maximum DCMD firing rate and the start co-contraction was 36 ms (SD: 23).

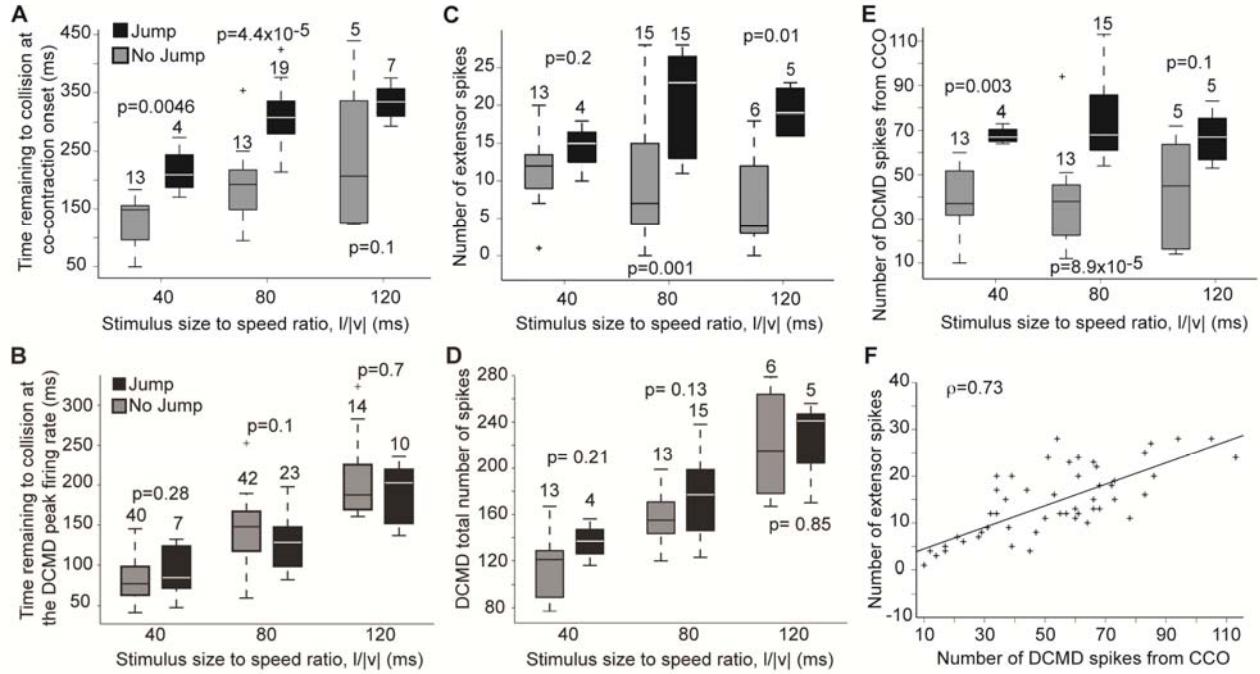


Figure 10. Comparison between sensory and motor activity in Jump (J) and No Jump (NJ) trials. **A)** Co-contraction started earlier in J trials. **B)** Timing of the DCMD peak rate was not significantly different in J and NJ trials. **C)** The number of extensor spikes was higher and did not change significantly with  $l/v$  ( $p_{\text{KWT-J}} = 0.18$ ,  $p_{\text{KWT-NJ}} = 0.15$ ). **D)** The total number of DCMD spikes was not significantly different in J and NJ trials. **E)** The number of DCMD spikes from Co-Contraction Onset (CCO) was higher in J trials and did not change significantly with  $l/v$  ( $p_{\text{KWT-J}} = 0.6$ ,  $p_{\text{KWT-NJ}} = 0.9$ ). **F)** In both J and NJ trials the number of extensor spikes from CCO was positively correlated with the number of DCMD spikes (linear fit slope: 0.2, SD: 0.09; intercept: 2 spk, SD: 1.5). Kruskal-Wallis test p values and  $n_T$  shown on plots. Data from 4 locusts (except **B**, where  $n_L = 10$ ).

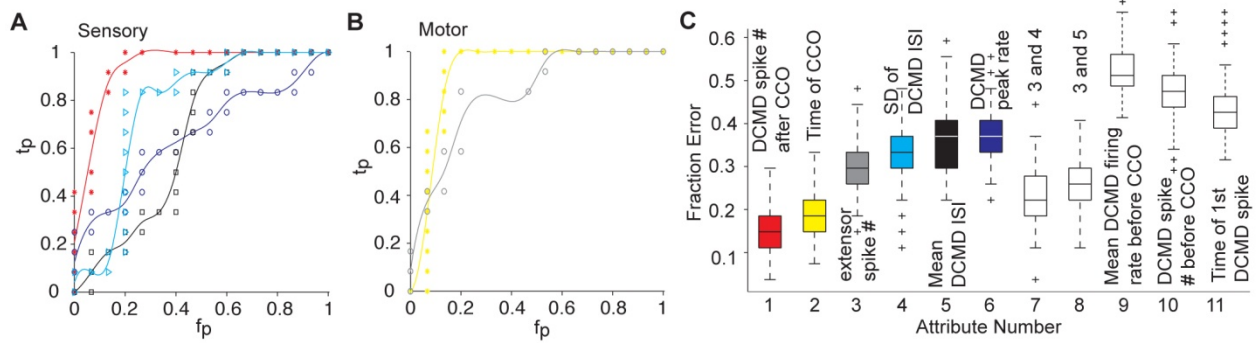


Figure 11. Predicting take-off from sensory and motor attributes. **A)** Receiver Operating Characteristics (ROC) curve for naïve Bayes classifiers trained to distinguish between Jump (J) and No Jump (NJ) trials based on the number of DCMD spikes (red), the SD of the DCMD ISI (cyan), the mean DCMD ISI (black), and the DCMD peak firing rate (blue). Abbreviations:  $t_p$  = true positives,  $f_p$  = false positives. **B)** ROC curve for classifiers trained with the timing of co-contraction onset (CCO, yellow) and the number (#) of extensor spikes (gray). **C)** Misclassification rate of different classifiers trained and tested with 100 random data shuffles. Chance level: 0.5. Attributes are as follows (including medians in J and NJ trials and difference significance level): 1: Number of DCMD spikes from CCO (J: 67, NJ: 38,  $p_{\text{KWT}}: 9.4 \times 10^{-8}$ ); 2: Time of CCO relative to projected collision (J: 307 ms, NJ: 152,  $p_{\text{KWT}}: 4.4 \times 10^{-7}$ ); 3: Number of extensor spikes (J: 20, NJ: 10,  $p_{\text{KWT}}: 3.2 \times 10^{-5}$ ); 4: SD of DCMD ISI after CCO (J: 2 ms, NJ: 3,  $p_{\text{KWT}}: 0.0141$ ); 5: Mean DCMD ISI after CCO (J: 3 ms, NJ: 4,  $p_{\text{KWT}}: 4.0 \times 10^{-3}$ ); 6: DCMD peak firing rate (J: 427 spk/s, NJ: 362,  $p_{\text{KWT}}: 1.9 \times 10^{-3}$ ); 9: Mean DCMD firing rate before CCO (J: 34 spk/s, NJ: 32,  $p_{\text{KWT}}: 0.74$ ); 10: number of DCMD spikes before CCO (J: 112, NJ: 105,  $p_{\text{KWT}}: 0.15$ ); 11: Time of 1st DCMD spike from stimulus onset (J: 3923 ms, NJ: 3564,  $p_{\text{KWT}}: 0.06$ ).

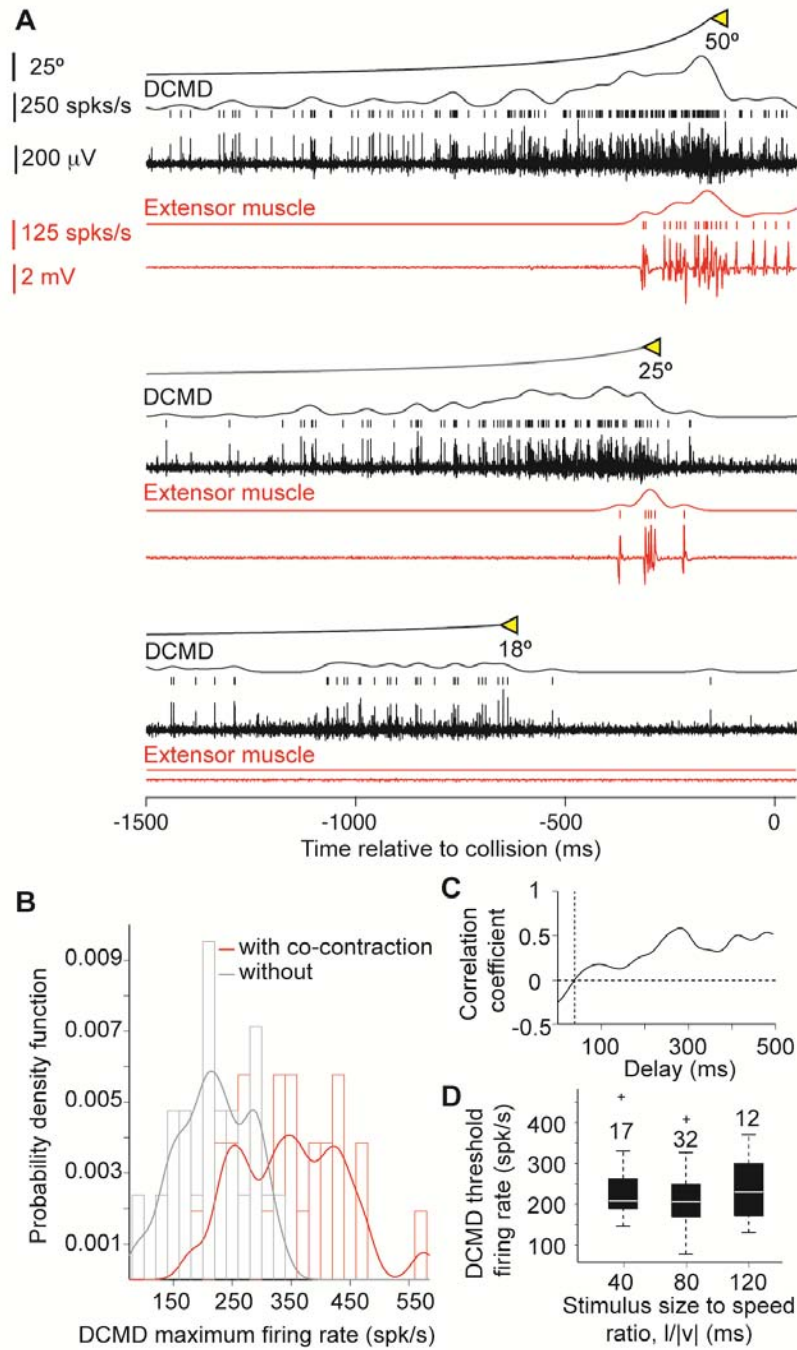


Figure 12. A DCMD firing rate threshold contributes to triggering co-contraction. **A**) Example of neural and muscle recordings in response to looming stimuli with three final angular sizes (18, 25 and 50°;  $l/|v|=80$  ms). As the final size increases the DCMD maximum firing rate and the total number of extensor spikes increase as well. For a final size of 18°, the co-contraction did not occur. **B**) Probability Density Function (PDF) for the DCMD maximum firing rate in the trials with, and without co-contraction (red and gray, respectively). The PDF is estimated using a non-parametric fit to the firing rate histogram as the sum of Gaussian kernels with bandwidths equal to 20 spk/s. **C**) Correlation coefficient between the DCMD firing rate and  $l/|v|$  plotted as a function of the delay before co-contraction onset. The correlation coefficient equals zero 40 ms before co-contraction onset. **D**) At that time the DCMD firing rate does not depend on  $l/|v|$  ( $p_{\text{KWT}} = 0.6$ ), and has an average value of 225 spk/s (SD: 73). Data from 4 locusts presented with full-expansion looming stimuli.

As a third approach for assessing the role of a DCMD firing rate threshold in triggering co-contraction, we carried out a correlation analysis on the data recorded in trials with full stimulus expansion. We hypothesized that if the co-contraction is triggered a fixed delay after a threshold DCMD firing rate is reached, the value of the firing rate at that delay must be independent of  $1/|v|$ . Consistent with this hypothesis, the DCMD firing rate and the stimulus size to speed ratio were uncorrelated 40 ms prior to co-contraction onset (Fig. 12C). The firing rate at this delay did not significantly change with  $1/|v|$  ( $p_{\text{KWT}}=0.6$ ) and had an average of 225 spk/s (SD: 73; Fig. 12D), close to the values predicted by the two other methods considered above. Taking into account the observed variability, we conclude that the co-contraction is triggered approximately 40 ms after the DCMD approximately exceeds a firing rate of 250 spk/s.

Using data from the same experiments, we next checked that the total number of DCMD spikes from trial start to co-contraction onset was only weakly correlated with the time of co-contraction ( $\rho = 0.07$ ,  $p = 0.6$ ). This result is also consistent with a change in DCMD firing rate immediately before co-contraction onset, such as a firing rate threshold, being more critical than accumulation of spikes over the entire trial. The trial-by-trial correlation of the firing rate threshold time with that of co-contraction onset was high ( $\rho = 0.6$ ,  $p < 10^{-9}$ ) and predicted 36% of the variance of co-contraction onset. Furthermore, this correlation value decreased by 1/3 when we randomly shuffled these two variables across trials ( $\rho = 0.39$ ,  $p = 0.01$ ; mean over 100 shuffles, SD: 0.07) and was significantly smaller than that obtained without shuffling ( $p = 0.001$ , z-test). These results also suggest that a DCMD firing rate threshold plays a trial-by-trial role in determining the onset of co-contraction, but that other neurons may contribute as well.

To quantify the steepness of the threshold, we plotted the extensor firing rate as a function of the DCMD firing rate and computed the DCMD firing rate change resulting in the extensor sweeping from 5 to 25% of its peak rate. On average the corresponding relative DCMD firing rate change amounted to ~5% and was thus approximately 4 times steeper than that of the extensor (20%).

### Recording from Loosely-Tethered Flying Locust

We have begun investigations to detail the mechanisms of collision avoidance in flying animals. For this purpose we set up a wind tunnel, two recording cameras to track the animals as they fly and a video projector which together with a rear projection screen allows us to present looming stimuli to the animals (Fig. 13).

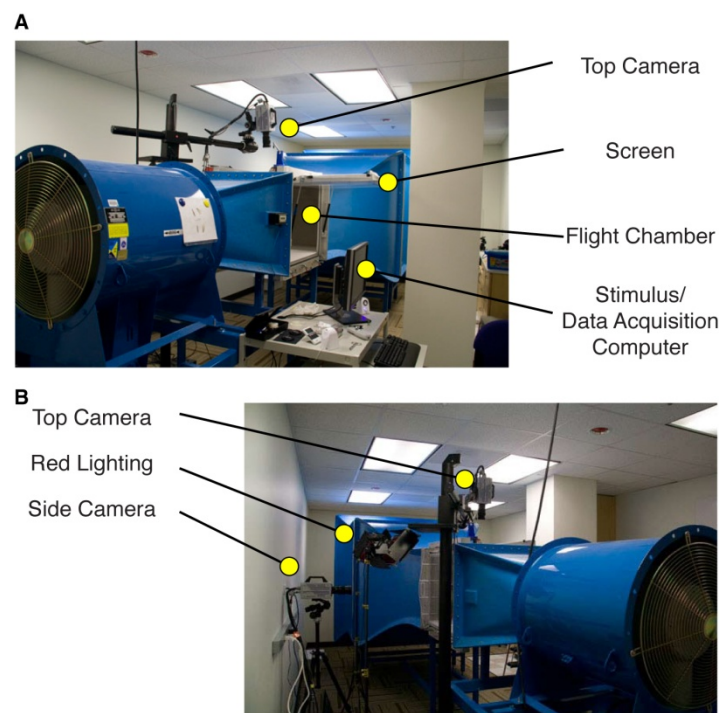


Figure 13. Side views of the wind tunnel and of the equipment used to film the animals. **A.** Left view (relative to the direction of wind flow) showing the position of the projection screen on the side opening of the test chamber, the top camera and the data acquisition computer. **B.** Right view showing the second camera and lightening equipments. We typically use red light as it is not perceived through the motion detecting pathways of the animal.

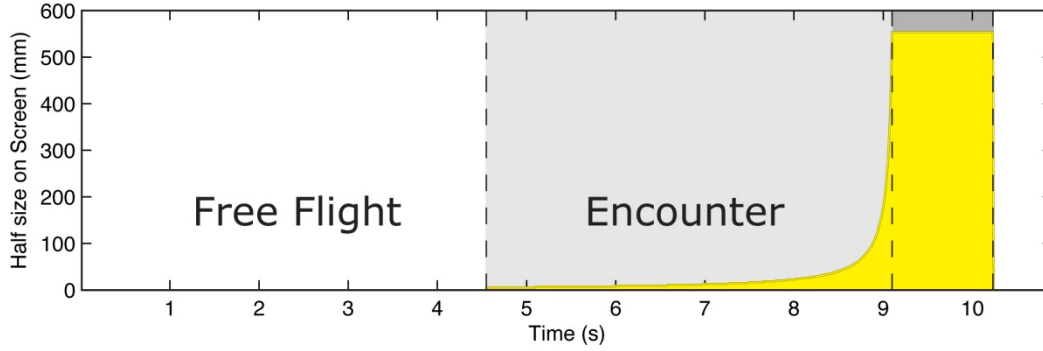


Figure 14. Stimuli generated on the rear projection screen simulate the approach of a disc on a collision course. They are referred to as looming stimuli. The x-axis represents time during a trial and the y-axis the size of the object on the screen.

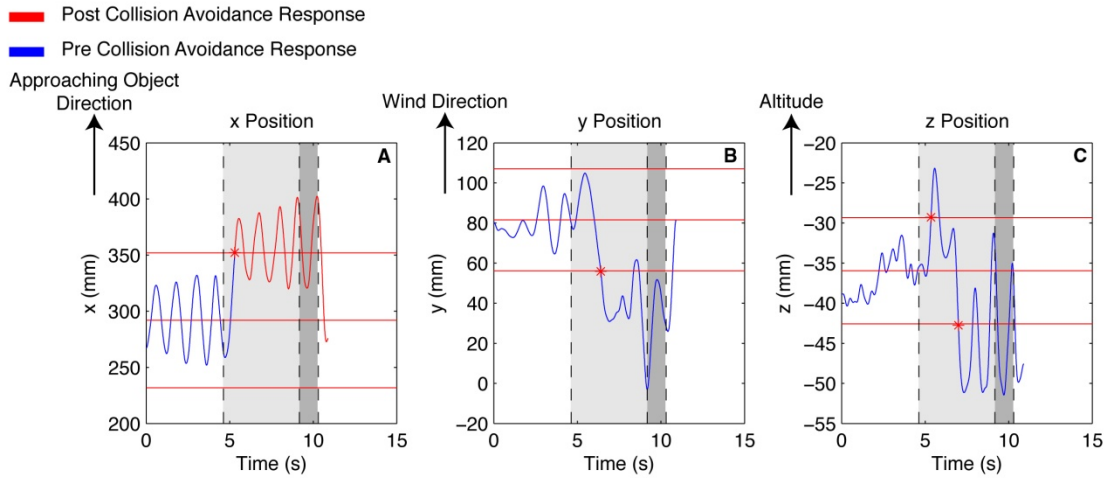


Figure 15. Animal's trajectory during a looming stimulus presentation. **A** depicts the animal's position along the direction of object approach. In this case the animal is steering away from the object. The top and bottom red lines denote the boundaries used to define collision avoidance behaviors and the gray shaded areas refer to the epochs of Fig. 14. **B** illustrates the trajectory in the direction of wind flow and **C** the trajectory in the vertical direction.

The time course of an experiment is schematized in Fig. 14. We record a movie of the animal during free-flight at a rate of 500 images/s during 4.5 s. Next, a looming stimulus is presented to the animal ("encounter") and at the end of its expansion an additional second of data is acquired. Following an experiment, the three-dimensional trajectory of the animal is reconstructed from the video images along the three cardinal axes of the flight chamber (Fig. 15). We consider that a collision avoidance behavior has occurred when the animal's trajectory crosses a boundary along each of the axes that is defined as twice the maximal excursion of the animal along that axis during free flight. An alternative representation consists in plotting two-dimensional projections of the trajectory, as illustrated in Fig. 16. Such plots show that the animal steered away from the object, dived and increased its flight speed. The simultaneous use of several escape strategies was typical of our subjects, as illustrated in Fig. 17.

Fig. 18 illustrates the timing of the collision avoidance behaviors relative to the stimulus epochs, showing that they typically occur during the object approach sequence. We are currently investigating the aerodynamical mechanisms underlying the collision avoidance behaviors. Fig. 19 illustrates one example, where we can clearly identify a wing flapping asymmetry in the forewings around the time of the collision avoidance behavior, suggesting that this change in wing kinematics may be responsible for the collision avoidance behavior.

These preliminary results show that we can reliably generate collision avoidance behaviors in the wind tunnel and analyze their properties in view of relating them to the neural activity generated by the DCMD neuron. We have used the wireless telemetry system in preliminary experiments to observe wing muscle EMGs (and corresponding body acceleration) during loosely tethered flight in a low-speed wind tunnel (see Fig. 20). Muscle activity in the right and left wing depressor muscles occurs in synchrony with the wing beats (and corresponding body acceleration) at approximately 18 Hz during flight (see Fig. 21).

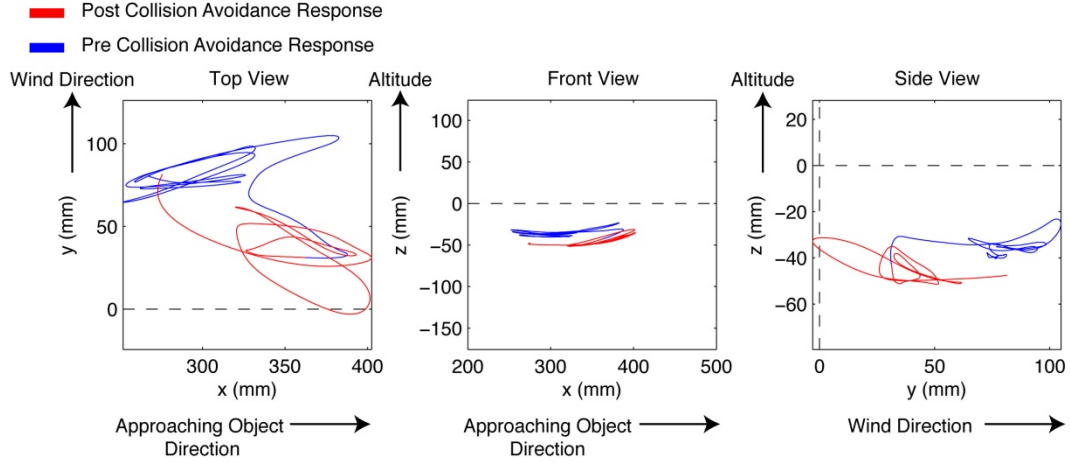


Figure 16. Two dimensional plots of the animal's trajectory along all three subset of cardinal axes. Same experiment as in Fig. 15.

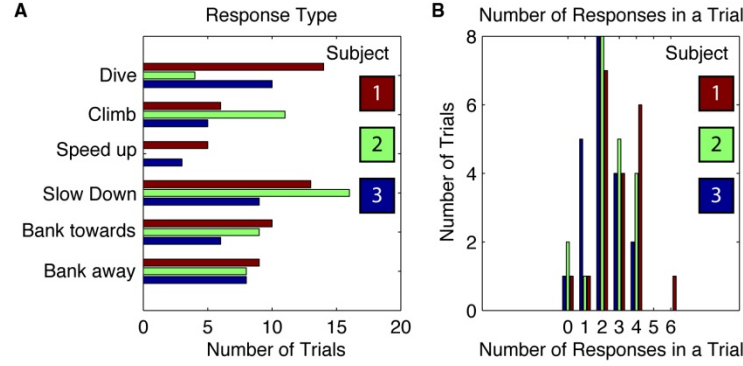


Figure 17. **A.** Histogram of the collision avoidance behaviors generated by three locusts that were presented repeatedly with looming stimuli. The possible escape behaviors are bank away or towards the stimulus, speed up or slow down and climb or dive. **B.** Histogram of the number of responses simultaneously generated by a locust during a single trial. The majority of trials contain more than one collision avoidance behavior.

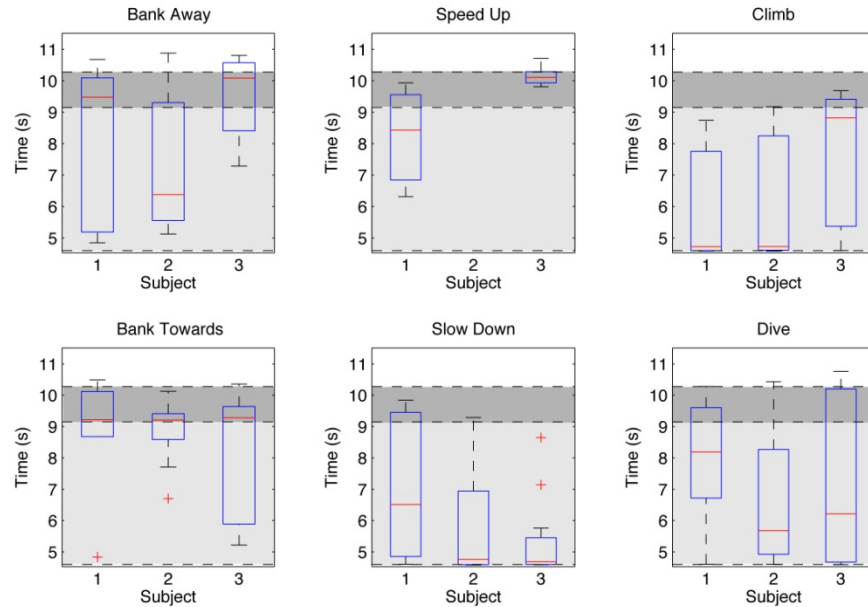


Figure 18. Time at which the six different types of collision avoidance behaviors occur during a trial. The gray shaded areas refer to the stimulus epochs defined in Fig. 14. Each box plot represents the median (red line), the 25 and 75 percentiles of the data (blue) and the extent of the data (black whiskers). Red crosses are outliers. The response times are given independently for the three subjects tested.

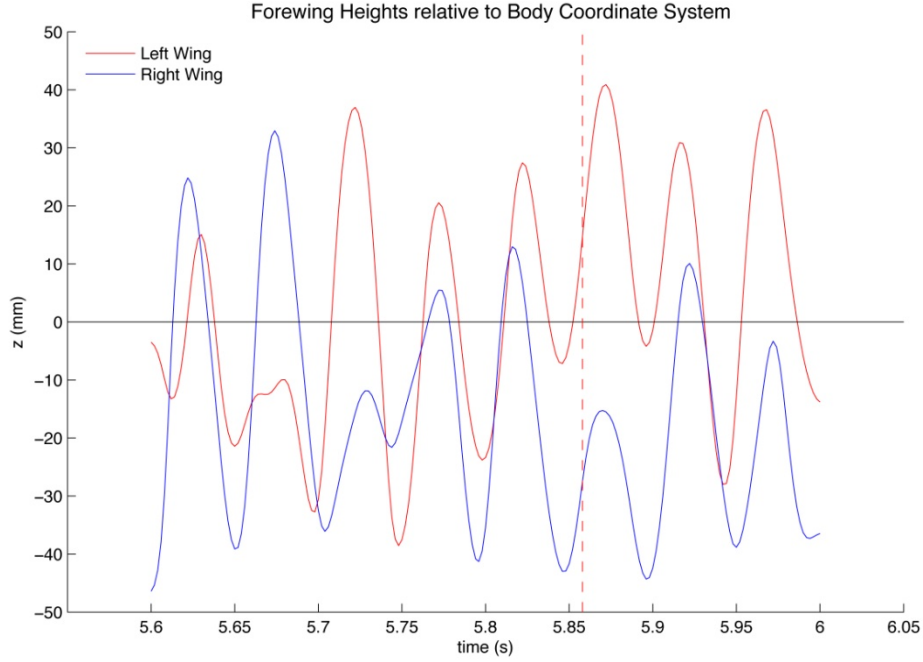


Figure 19. Trajectory of the left and right forewing tips in the vertical plane around the time of a collision avoidance behavior (vertical dashed red line).



Figure 20. Photograph of live wireless data acquisition from locust flying in wind tunnel. Wing beats are visible in EMG traces (center, left of finger). High-speed video of locust is synchronized to telemetry data.

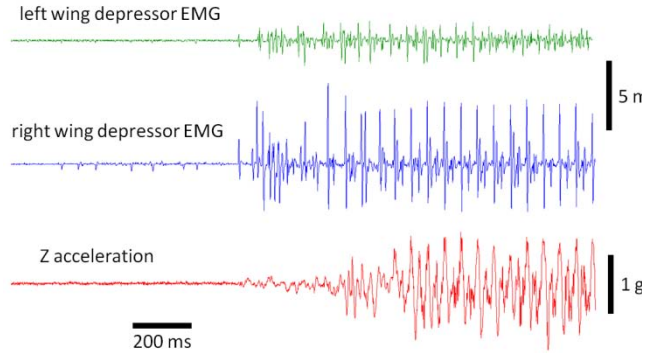


Figure 21. Data obtained wirelessly from a loosely tethered locust flying in a wind tunnel. Onset of 18 Hz wing beats is observed in the two wing EMG traces (top) and acceleration trace (bottom).

#### IV. DISCUSSION

Using a novel miniature telemetry system, we were for the first time able to record simultaneously the sensory and motor activity contributing to the execution of a complex, multi-stage escape behavior in freely behaving animals. Our results suggest that the DCMD neuron contributes to multiple aspects of this behavior through several distinct attributes of its time-varying firing rate.

As collision becomes imminent, the DCMD plays an increasingly important role in the preparatory events leading to the jump. Thus, early on, we found little evidence for an involvement of the DCMD in the initial preparatory movements. Indeed, animals with a sectioned nerve cord still carried them out, albeit with increased variability.

Timely start of energy storage, through co-contraction of flexors and extensors, was critical for the successful execution of escape responses (Fig. 10A). In experiments where looming stimuli stopped at different final sizes, a DCMD firing rate threshold accurately predicted the occurrence of co-contraction. However, only 36% of the variance of co-contraction onset in experiments with the largest final angular size could be predicted from that of the DCMD firing rate threshold on a trial-by-trial basis. This suggests that other neurons play important roles as well. In the meta-thoracic ganglion, the DCMD makes bilateral excitatory connections with the FETi motoneuron (Hoyle and Burrows, 1973). The DCMD also makes excitatory connections with the C interneuron, which in turn co-excites the FETi and flexor motoneurons, and is thought to play an important role in triggering co-contraction (Pearson and Roberston, 1981). Proprioceptive feedback also affects its onset (Burrows and Pflüger, 1988). Therefore, our findings about the role of the DCMD in triggering co-contraction and take-off are consistent with its known anatomical connections with the downstream motor circuitry.

After the start of co-contraction, we found a very strong correlation between the number of DCMD and extensor spikes (Fig. 10C). Moreover, this correlation was higher for trials with a smaller mean DCMD ISI, suggesting that the summation of DCMD-evoked EPSPs in the FETi motor neuron occurs more reliably. Finally, the FETi firing rate followed faithfully that of the DCMD. Thus, co-contraction onset appears to act as a *switch* that triggers faithful transmission of DCMD spikes to the FETi motoneuron. Previously, DCMD spikes alone have been thought incapable of generating spikes in the FETi motoneuron (Burrows and Rowell, 1973; Rogers et al., 2007). In those studies, the peak DCMD firing rate was however lower than the threshold we report for triggering co-contraction. The DCMD neuron was more active in our experiments most likely due to: (i) increased arousal in freely behaving animals (Rowell, 1971b); (ii) increased ambient temperature; (iii) pre-selection of locusts that responded readily to looming stimuli (typically one third of the animals). Additionally, the EPSPs from the DIMD presumably summated with those of the DCMD (Burrows and Rowell, 1973).

We could predict 75% of the trial-to-trial variability of the jump time from the DCMD peak firing time. The remaining variability could be due to activation of other neurons by the DCMD, such as the bilaterally paired M interneurons, which are thought to contribute to the inhibition of the flexor motoneurons (Pearson et al., 1980). The time course of the decay in firing rate of the DCMD following its peak, which likely contributes to the end of co-contraction (Fotowat and Gabbiani, 2007), could also contribute to the variability in the take-off time. Other sources of variability could be the DIMD, other ipsi and contralateral descending looming sensitive neurons, other local interneurons, and sensory feedback from leg proprioceptors (Gynther and Pearson 1989; Jellema and Heitler, 1999).

Finally, we found that the number of DCMD spikes from co-contraction onset was highly predictive of jump occurrence. A classifier trained on the number of DCMD spikes from co-contraction onset performed even better than one trained on the number of extensor spikes. This points to the fact that the DCMD activity controls jump execution not only through activation of the leg extensor motor neurons, but also through other factors, such as the onset of flexor inhibition, for example.

In conclusion, the transformation of sensory activity into the motor program leading to jump in response to looming stimuli relies at least on three distinct attributes of a single neuron's time-varying discharge: a firing rate threshold, the peak firing rate time and the number of spikes from a specific trigger event (co-contraction onset). This 'multiplexing' of motor-related information in a sensory neuron's response could not be evidenced in earlier experiments where behavior and electrophysiology were carried out separately (Fotowat and Gabbiani, 2007). Recently, the generation of a few spikes in a single neuron, or of single spikes in a sparse set of neurons, was shown to be capable of producing behavior in rodents (Houweling and Brecht, 2008; Huber et al., 2008). It is not known, however, how the time-course of these neuronal activities correlates with the observed behavior. Working in a system where much of the implicated neuronal circuitry has been identified allowed us to study how visual responses contribute to distinct motor phases of an ongoing behavior. Moreover, we could study how variability in the sensory response affects the final motor output on a trial-by-trial basis. We expect that miniature wireless telemetry will contribute to the study of sensorimotor integration during free behavior in other species as well.

Table II summarizes the measured performance of the miniature wireless telemetry system. Fig. 22 shows the custom RF receiver with USB interface built to collect the wireless data. An audio port allows for real-time monitoring of neural or EMG signals over headphones during experiments. The small size and low mass of this device will enable new experiments in the study of the neural control of behavior.

TABLE II. TELEMETRY TRANSMITTER MEASURED PERFORMANCE

Supply voltage	3.0 V
Supply current (chip only, without accelerometer)	0.88 mA
Supply current (complete system, with accelerometer)	1.2 mA
Transmit frequency	920 MHz
FSK modulation depth	600 kHz
Telemetry data rate	345.6 kb/s
Telemetry range (using low-gain, omnidirectional receive antenna)	~2 m
Total system mass (including PCB, accelerometer, crystal, batteries)	0.79 g
Battery life	2 h

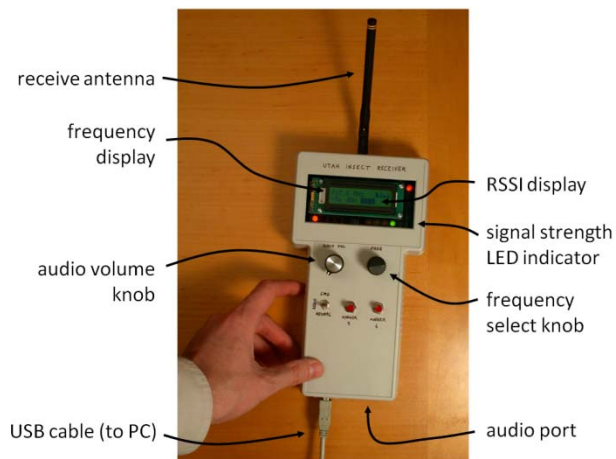


Figure 22. Custom wireless telemetry receiver with USB interface to PC.

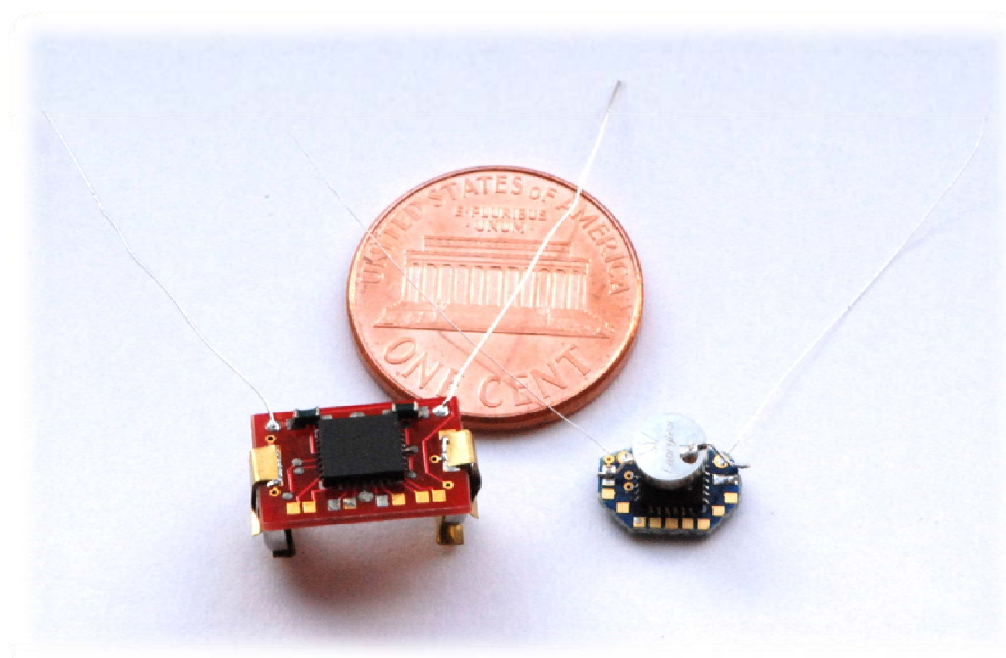


Figure 23. First-generation wireless telemetry system weighing 790 mg (left); next-generation system weighing 266 mg (right).

## V. NEXT-GENERATION WIRELESS RECORDING SYSTEM

With the assistance of additional funding from the Howard Hughes Medical Institute's Janelia Farm Research Campus (JFRC), we developed a next-generation wireless recording system that is much smaller and lighter than the first-generation system used in the experiments shown above. This new system, shown in Fig. 23, is being phased into wind tunnel experiments at Baylor. The second-generation chip runs from a 1.5-V supply, requiring only one Energizer 337 battery. While the new chip transmits two neural and two EMG signals as the original chip, no commercial accelerometers work below 1.8 V, so acceleration signals are not available on the new telemetry system. This new system was finalized in 2010.

## VI. REFERENCES

- Burrows, M. (1996). *The Neurobiology of an insect brain* (Oxford: Oxford University Press).
- Burrows, M. (1987). Parallel processing of proprioceptive signals by spiking local interneurons and motor neurons in the locust. *J. Neurosci.* 7, 1064–1080.
- Burrows, M. and Rowell, C. F. (1973). Connections between descending visual interneurons and metathoracic motoneurons in the locust. *J. Comp. Physiol.* 85, 221–234.
- Burrows, M. and Pflüger, H. (1988). Positive feedback loops from proprioceptors involved in leg movements of the locust. *J. Comp. Physiol. A* 163, 425–440.
- Camhi, J. M. and Levy, A. (1989). The code for stimulus direction in a cell assembly in the cockroach. *J. Comp. Physiol. A* 165, 83–97.
- Cohen, M. R. and Newsome, W. T. (2009). Estimates of the contribution of single neurons to perception depend on timescale and noise correlation. *J. Neurosci.* 29, 6635–48.
- Cook, E. P. and Maunsell, J. H. R. (2002). Dynamics of neuronal responses in macaque mt and vip during motion detection. *Nat. Neurosci.* 5, 985–94.
- Daly, D.C., Mercier, P.P., Bhardwaj, M., Stone, A.L., Voldman, J., Levine, R.B., Hidebrand, J.G., and Chandrakasan, A.P. (2009). A pulsed UWB receiver SoC for insect motion control, *ISSCC Dig. Tech. Papers*, 200–201, Feb. 2009.
- de Lafuente, V. and Romo, R. (2005). Neuronal correlates of subjective sensory experience. *Nat. Neurosci.* 8, 1698–703.
- Edwards, D. H., Heitler, W. J. and Krasne, F. B. (1999). Fifty years of a command neuron: the neurobiology of escape behavior in the crayfish. *Trends Neurosci.* 22, 153–61.
- Farrow, K., Haag, J. and Borst, A. (2003). Input organization of multifunctional motion-sensitive neurons in the blowfly. *J. Neurosci.* 23, 9805–9811.
- Fotowat, H., Fayyazuddin, A., Bellen, H. J. and Gabbiani, F. (2009). A novel neuronal pathway for visually guided escape in drosophila melanogaster. *J. Neurophysiol.* 102, 875–85.
- Fotowat, H. and Gabbiani, F. (2007). Relationship between the phases of sensory and motor activity during a looming-evoked multistage escape behavior. *J. Neurosci.* 27, 10047–59.
- Gabbiani, F., Krapp, H. G. and Laurent, G. (1999). Computation of object approach by a wide-field, motion-sensitive neuron. *J. Neurosci.* 19, 1122–41.
- Fotowat, H., Harrison, R.R., and Gabbiani, F. (2009). Measuring neural correlates of insect escape behaviors using a miniature telemetry system, In: *Proc. 35th Annual Northeast Bioengineering Conf.*, Cambridge, MA.
- Gabbiani, F., Mo, C. and Laurent, G. (2001). Invariance of angular threshold computation in a wide-field looming-sensitive neuron. *J. Neurosci.* 21, 314–329.
- Gabbiani, F., Krapp, H.G., Koch, C. and Laurent, G. (2002). Multiplicative computation in a visual neuron sensitive to looming. *Nature* 21, 320–324.
- Gabbiani, F., Cohen, I. and Laurent, G. (2005). Time-dependent activation of feed-forward inhibition in a looming-sensitive neuron. *J. Neurophysiol.* 94, 2150–2161.
- Graziano, M., Andersen, R. and Snowden, R. (1994). Tuning of mst neurons to spiral motions. *J. Neurosci.* 14, 54–67.
- Gu, Y., Angelaki, D.E. and Deangelis, G.C. (2008). Neural correlates of multisensory cue integration in macaque MSTd. *Nat. Neurosci.* 11, 1201–10.
- Gynther, I. C. and Pearson, K. G. (1989). An evaluation of the role of identified interneurons in triggering kicks and jumps in the locust. *J. Neurophysiol.* 61, 45–57.
- Harrison, R.R. and Charles, C. (2003). A low-power, low-noise CMOS amplifier for neural recording applications, *IEEE J. Solid-State Circuits*, 38, 958–965, June 2003.

- Harrison, R.R. (2008). The design of integrated circuits to observe brain activity, *Proc. of the IEEE*, 96, 1203-1216, July 2008.
- Hatsopoulos, N., Gabbiani, F. and Laurent, G. (1995). Elementary computation of object approach by wide-field visual neuron. *Science* 270, 1000-3.
- Heitler, W. J. (1995). Quasi-reversible photo-axotomy used to investigate the role of extensor muscle tension in controlling the kick motor programme of grasshoppers. *Eur. J. Neurosci.* 7, 981-992.
- Houweling, A. R. and Brecht, M. (2008). Behavioural report of single neuron stimulation in somatosensory cortex. *Nature* 451, 65-8.
- Hoyle, G. (1978). Distributions of nerve and muscle fibre types in locust jumping muscle. *J. Exp. Biol.* 73, 205-233.
- Huber, D., Petreanu, L., Ghitani, N., Ranade, S., Hromádka, T., Mainen, Z. and Svoboda, K. (2008). Sparse optical microstimulation in barrel cortex drives learned behaviour in freely moving mice. *Nature* 451, 61-4.
- Ishikane, H., Gangi, M., Honda, S. and Tachibana, M. (2005). Synchronized retinal oscillations encode essential information for escape behavior in frogs. *Nat. Neurosci.* 8, 1087-1095.
- Jacobs, G. A. and Miller, J. P. (1985). Functional properties of individual neuronal branches isolated in situ by laser photoinactivation. *Science* 228, 344-346.
- Jellema T. and Heitler, W. J. (1999). Central and peripheral control of the trigger mechanism for kicking and jumping in the locust. *J. Comp. Neurol.* 404, 212-20.
- Judge, S. and Rind, F.C. (1997). The locust DCMD, a movement-detecting neurone tightly tuned to collision trajectories. *J. Exp. Biol.* 200, 2209-2216.
- Kang, H. and Nakagawa, H. (2006). Collision-sensitive neurons in the optic tectum of the bullfrog (*rana catesbeiana*). *Int. Congr. Series* 1291, 145-148.
- Killmann, F. and Schurmann, F. (1985). Both electrical and chemical transmission between the 'lobula giant movement detector' and the 'descending contralateral movement detector' neurons of locusts are supported by electron microscopy. *J. Neurocytol.* 14, 637-652.
- Korn, H. and Faber, D. S. (2005). The mauthner cell half a century later: a neurobiological model for decision-making? *Neuron* 47, 13-28.
- Kutsch, W., Schwarz, G., Fischer, H., and Kautz, H. (1993). Wireless transmission of muscle potentials during free flight of a locust, *J. Exp. Biol.*, 185, 367-373.
- Kuwana Y., Ando N., Kanzaki, R., and Shimoyama, I. (1999). A radiotelemetry system for muscle potential recordings from freely flying insects, In: *Proc. BMES/EMBS Conf.*, vol. 2, 846, Oct. 1999.
- Lewis, J. E. and Kristan, W. B. Jr. (1998). A neuronal network for computing population vectors in the leech. *Nature* 391, 76-79.
- Lima, S. Q. and Miesenböck, G. (2005). Remote control of behavior through genetically targeted photostimulation of neurons. *Cell* 121, 141-52.
- Liu, K. S. and Fetcho, J. R. (1999). Laser ablations reveal functional relationships of segmental hindbrain neurons in zebrafish. *Neuron* 23, 325-335.
- Marsat, G. and Pollack, G. S. (2006). A behavioral role for feature detection by sensory bursts. *J. Neurosci.* 26, 10542-7.
- Mavoori, J., Millard, B., Longnion, J., Daniel, T., and Diorio, C., A miniature implantable computer for functional electrical stimulation and recording of neuromuscular activity, In: *Proc. IEEE Intl. Workshop Biomedical Circuits and Systems*, pp. 13-16, Dec. 2004.
- Miller, J. P. and Selverston, A. (1979). Rapid killing of single neurons by irradiation of intracellularly injected dye. *Science* 206, 702-704.
- Mountcastle, V. B., Lynch, J. C., Georgopoulos, A., Sakata, H. and Acuna, C. (1975). Posterior parietal association cortex of the monkey: command functions for operations within extrapersonal space. *J. Neurophysiol.* 38, 871-908.

- Newsome, W. T., Wurtz, R. H. and Komatsu, H. (1988). Relation of cortical areas MT and MST to pursuit eye movements. ii. differentiation of retinal from extraretinal inputs. *J Neurophysiol.* 60, 604–20.
- Nienborg, H. and Cumming, B. G. (2009). Decision-related activity in sensory neurons reflects more than a neuron's causal effect. *Nature* 459, 89–92.
- Olberg, R., Seaman, R.C., Coats, M.I., and Henry, A.F. (2007). Eye movements and target fixation during dragonfly prey interception flights, *J. Comp. Phys. A*, 193, 685-693.
- Oliva, D., Medan, V. and Tomsic, D. (2007). Escape behavior and neuronal responses to looming stimuli in the crab chasmagnathus granulatus (decapoda: Grapsidae). *J. Exp. Biol.* 210, 865–80.
- O'Shea, M., Rowell, C. and Williams, J. (1974). The anatomy of a locust visual interneurone; the descending contralateral movement detector. *J. Exp. Biol.* 60, 1–12.
- Pearson, K. G., Heitler, W. J. and Steeves, J. D. (1980). Triggering of locust jump by multimodal inhibitory interneurons. *J. Neurophysiol.* 43, 257–78.
- Pearson, K. and Robertson, R. (1981). Interneurons coactivating hindleg flexor and extensor motoneurons in the locust. *J. Comp. Physiol. A* 144, 391–410.
- Peron, S. and Gabbiani, F. (2009). Spike frequency adaptation mediates looming stimulus selectivity in a collision-detecting neuron. *Nat. Neurosci.* 12, 318–26.
- Preuss, T., Osei-Bonsu, P. E., Weiss, S. A., Wang, C. and Faber, D. S. (2006). Neural representation of object approach in a decision-making motor circuit. *J. Neurosci.* 26, 3454–64.
- Rind, F. C. (1984). A chemical synapse between two motion detecting neurones in the locust brain. *J. Exp. Biol.* 110, 143–67.
- Rind, F.C. and Simmons, P. (1992). Orthopteran dcmd neuron: a reevaluation of responses to moving objects. I. selective responses to approaching objects. *J. Neurophysiol.* 68, 1654–1666.
- Rogers, S. M., Krapp, H. G., Burrows, M. and Matheson, T. (2007). Compensatory plasticity at an identified synapse tunes a visuomotor pathway. *J. Neurosci.* 27, 4621–33.
- Roitman, J. D. and Shadlen, M. N. (2002). Response of neurons in the lateral intraparietal area during a combined visual discrimination reaction time task. *J. Neurosci.* 22, 9475–89.
- Rowell, C. (1971). The orthopteran descending movement detector (dmd) neurones: a characterisation and review. *J. Comp. Physiol. A* 73, 167–194.
- Rowell, C. (1971b). Variable responsiveness of a visual interneurone in the free-moving locust, and its relation to behaviour and arousal. *J. Exp. Biol.* 55, 727–747.
- Santer, R., Rind, F.C., Stafford, R. and Simmons, P. (2006). Role of an identified looming-sensitive neuron in triggering a flying locust's escape. *J. Neurophysiol.* 95, 3391–3400.
- Santer, R. D., Yamawaki, Y., Rind, F. C. and Simmons, P. J. (2005). Motor activity and trajectory control during escape jumping in the locust *Locusta migratoria*. *J. Comp. Physiol. A* 191, 965-975.
- Santer, R. D., Yamawaki, Y., Rind, F. C. and Simmons, P. J. (2008). Preparing for escape: an examination of the role of the dcmd neuron in locust escape jumps. *J. Comp. Physiol. A* 194, 69–77.
- Schlotterer, G. R. (1977). Response of the locust descending movement detector neuron to rapidly approaching and withdrawing visual stimuli. *Canad. J. Zool.* 55, 1372–1376.
- Simmons, P. (1980). Connexions between a movement-detecting visual interneurone and flight motoneurons of a locust. *J. Exp. Biol.* 86, 87–97.
- Sun, H. and Frost, B. (1998). Computation of different optical variables of looming objects in pigeon nucleus rotundus neurons. *Nat. Neurosci.* 1, 296–303.
- Trimarchi, J. R. and Schneiderman, A. M. (1993). Giant fiber activation of an intrinsic muscle in the mesothoracic leg of *drosophila melanogaster*. *J. Exp. Biol.* 177, 149–67.

- van Hateren, J. H., Kern, R., Schwerdtfeger, G. and Egelhaaf, M. (2005). Function and coding in the blowfly H1 neuron during naturalistic optic flow. *J. Neurosci.* 25, 4343–52.
- Wang, Y. and Frost, B. J. (1992). Time to collision is signaled by neurons in the nucleus rotundus of pigeons. *Nature* 356, 236–8.
- Warzecha, A. K., Egelhaaf, M. and Borst, A. (1993). Neural circuit tuning fly visual interneurons to motion of small objects. I. Dissection of the circuit by pharmacological and photoinactivation techniques. *J. Neurophysiol.* 69, 329-339.
- Wicklein, M. and Strausfeld, N. J. (2000). Organization and significance of neurons that detect change of visual depth in the hawk moth *manduca sexta*. *J. Comp. Neurol.* 424, 356–76.
- Wikelski M., Moskowitz D., Adelman J.S., Cochran, J., Wilcove, D.S., and May, M.L. (2006). Simple rules guide dragonfly migration, *Biology Letters*, 2, 325-329.
- Yamamoto, K., Nakata, M. and Nakagawa, H. (2003). Input and output characteristics of collision avoidance behavior in the frog *rana catesbeiana*. *Brain. Behav. Evol.* 62, 201–11.

DISTRIBUTION LIST  
AFRL-RW-EG-TR-2010-110

DEFENSE TECHNICAL INFORMATION CENTER - 1 Electronic Copy (1 file & 1 format)  
ATTN: DTIC-OCA (ACQUISITION)  
8725 JOHN J. KINGMAN ROAD, SUITE 0944  
FT. BELVOIR VA 22060-6218

AFRL/RWOC (STINFO Office)	- 1 Hard (color) Copy
AFRL/RW CA-N	- STINFO Officer to provide notice of publication